5948–5960 *Nucleic Acids Research, 2022, Vol. 50, No. 10* *Published online 30 May 2022*
https://doi.org/10.1093/nar/gkac442

Molecular basis for cell-wall recycling regulation by transcriptional repressor MurR in *Escherichia coli*

Ya Zhang[1,2,†], Weizhong Chen[1,†], Di Wu[3,†], Yushi Liu[1], Zhaowei Wu[1], Jian Li[1], Shu-Yu Zhang[3,*] and Quanjiang Ji[1,4,*]

[1]School of Physical Science and Technology, ShanghaiTech University, Shanghai 201210, China, [2]University of Chinese Academy of Sciences, Beijing 100049, China, [3]Shanghai Key Laboratory for Molecular Engineer of Chiral Drugs, School of Chemistry and Chemical Engineering & Frontiers Science Center for Transformative Molecules, Shanghai Jiao Tong University, Shanghai 200240, China and [4]Gene Editing Center, School of Life Science and Technology, ShanghaiTech University, Shanghai 201210, China

Received January 11, 2022; Revised May 01, 2022; Editorial Decision May 09, 2022; Accepted May 10, 2022

ABSTRACT

The cell-wall recycling process is important for bacterial survival in nutrient-limited conditions and, in certain cases, is directly involved in antibiotic resistance. In the sophisticated cell-wall recycling process in *Escherichia coli*, the transcriptional repressor MurR controls the expression of *murP* and *murQ*, which are involved in transporting and metabolizing *N*-acetylmuramic acid (MurNAc), generating *N*-acetylmuramic acid-6-phosphate (MurNAc-6-P) and *N*-acetylglucosamine-6-phosphate (GlcNAc-6-P). Here, we report that both MurNAc-6-P and GlcNAc-6-P can bind to MurR and weaken the DNA binding ability of MurR. Structural characterizations of MurR in complex with MurNAc-6-P or GlcNAc-6-P as well as in the apo form revealed the detailed ligand recognition chemistries. Further studies showed that only MurNAc-6-P, but not GlcNAc-6-P, is capable of derepressing the expression of *murQP* controlled by *MurR* in cells and clarified the substrate specificity through the identification of key residues responsible for ligand binding in the complex structures. In summary, this study deciphered the molecular mechanism of the cell wall recycling process regulated by MurR in *E. coli*.

INTRODUCTION

The bacterial cell wall is an elastic macromolecule of bacterial architecture that defines cell shape and protects cells from lysis caused by intracellular turgor pressure (1). This macromolecule, also called the 'murein sacculus', is composed of tightly cross-linked peptidoglycan (PG) which varies in size and composition in different bacteria (2,3). In *Escherichia coli*, a typical gram-negative bacterium, the sacculus is composed of alternating *N*-acetylglucosamine (GlcNAc) and *N*-acetylmuramic acid (MurNAc)-pentapeptide linked by β-(1→4) glycosidic linkages (4–6). The pentapeptide on the lactyl moiety of MurNAc consists of L-alanine-γ-D-glutamate-mesodiaminopimelic acid-D-alanyl-D-alanine (L-Ala-γ-D-Glu-m-DAP-D-Ala-D-Ala) (7–9). Generally, cross-linking between two PG monomers is generated from the 3rd residue of one chain and the 4th residue of the other (5,10).

Cell-wall biosynthesis and recycling are inextricably coordinated for bacterial integrity. During the whole process of growth, elongation and division, bacteria recycle almost 40–50% of the cell-wall components per generation, which is critical for resource utilization (11–13). In addition, cell-wall recycling is also associated with bacterial antibiotic resistance (14–16). For instance, muropeptides, the breakdown products of the cell wall, were identified as signaling molecules that induce AmpC β-lactamase production. Cell wall recycling is an extremely sophisticated process that requires a large number of enzymes to cooperate with each other. In *E. coli*, the periplasmic amidases AmiA-D cut the peptide off from the muramyl moieties of the cell wall (17–20). Then the lytic transglycosylases (LTs), acting on the glycan strand of the peptidoglycan, cleave at the β-(1→4) glycosidic bond between the MurNAc and GlcNAc residues and release GlcNAc-anhMurNAc (21) (Figure 1). GlcNAc-anhMurNAc together with anhydromuropeptide (PG monomer) enters the cytoplasm through the AmpG permease where the peptide of the latter is snipped off by the cytosolic amidase AmpD (13,22,23) (Figure 1). The cytoplasmic *N*-acetylglucosaminidase NagZ hydrolytically cleaves the β-(1→4) glycosidic bond of the anhydrodisaccharides to generate GlcNAc and anhMurNAc, which is later phosphorylated by the anhydro-*N*-acetylmuramic acid

*To whom correspondence should be addressed. Tel: +86 21 2068 5480; Email: quanjiangji@shanghaitech.edu.cn
Correspondence may also be addressed to Shu-Yu Zhang. Tel: +86 21 5474 7808; Email: zhangsy16@sjtu.edu.cn
†The authors wish it to be known that, in their opinion, the first three authors should be regarded as Joint First Authors.

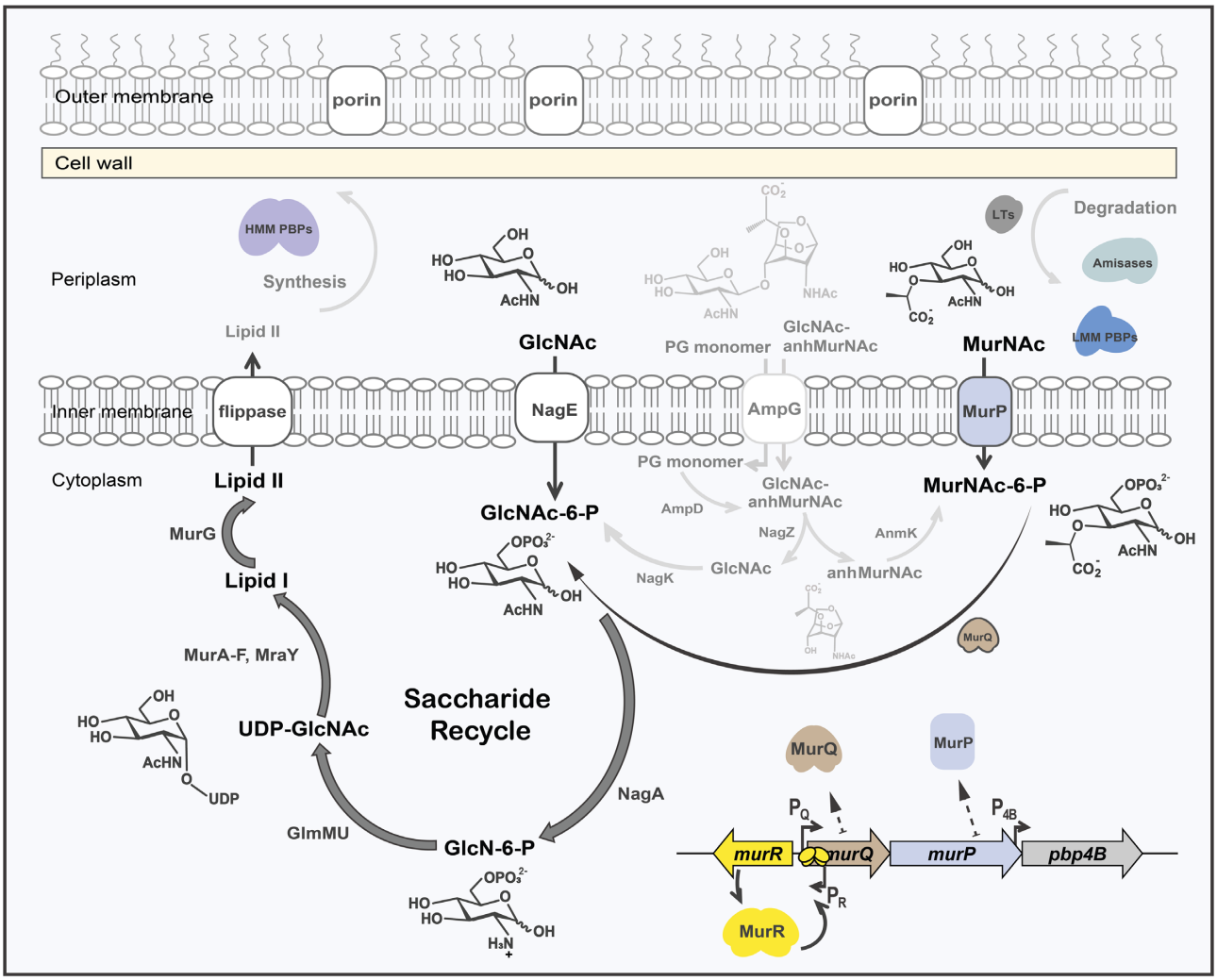

Figure 1. The graphic illustration of associated steps of saccharide recycle in cell-wall recycling in *Escherichia coli*. The cell wall breakdown products GlcNAc-anhMurNAc, PG monomer, MurNAc and GlcNAc enter into cytoplasm via specific channel protein AmpG, MurP and NagE, respectively. Phosphorylated MurNAc (MurNAc-6-P) is further metabolized by MurQ, yielding GlcNAc-6-P, which is deacetylated to GlcN-6-P by NagA. GlcN-6-P is then converted to UDP-GlcNAc by GlmMU. Then, MurA-F/MraY modify UDP-GlcNAc and produce lipid I, which is converted by MurG to the final intermediate lipid II. In this process, MurR controls the expressions of phosphotransferase MurP and etherase MurQ.

kinase AnmK to generate MurNAc-6-P (24–27). Together with the moiety entering via the MurNAc phosphotransferase MurP, MurNAc-6-P is further metabolized by the etherase MurQ, a specific hydrolase that cleaves the lactyl ether bond of MurNAc-6-P, yielding GlcNAc-6-P and D-lactate (28–30) (Figure 1). Following by deacetylation via NagA, the *N*-acetylglucosamine-6-phosphate deacetylase, the product of MurQ and NagE (31), is converted to glucosamine-6-phosphate (GlcN-6-P) (32). After isomerization to GlcN-1-P by GlmM (33), GlcN-6-P is linked with uridine-diphosphate (UDP) and acetyl-CoA by GlmU, yielding UDP-GlcNAc (34). Then, MurA-F/MraY mediate a series of reactions to convert UDP-GlcNAc to lipid I (MurNAc-pentapeptide with undecaprenyl pyrophosphate) (33,35,36), which is further converted to the final intermediate lipid II (GlcNAc-MurNAc-pentapeptide with undecaprenyl pyrophosphate) through GlcNAc linkage by MurG (37). Translocated by flippase, Lipid II provides the disaccharide-pentapeptide for *de novo* cell-wall synthesis (38).

MurR, a member of the poorly characterized RpiR/AlsR family transcription factors, functions as the specific repressor of *murQP*, whose translation products play a vital role in transporting and metabolizing MurNAc (39). In *E. coli*, MurR binds to two neighboring opposite repeats within the *murR-murQ* intergenic region, repressing the transcription of both *murQP* and itself (39) (Figure 1). MurNAc-6-P, the substrate of MurQ, is identified as a specific inducer, derepressing the expression of *murQP* by weakening the binding ability of MurR to the operator DNA (39). Compared with the wild-type strain, the *murR*-deletion mutant exhibits a faster growth rate in logarithmic phase when MurNAc is used as the sole carbon source (39). However, the molecular mechanism of this regulatory pathway remains unclear.

In this work, we revealed that MurNAc-6-P directly binds to MurR to induce the dissociation of MurR from the promoter DNA, leading to the derepression of the *murPQ* pathway. In addition, we found that another intermediate of amino sugar metabolism, GlcNAc-6-P, could also interact with MurR but with a lower binding affinity and weaker DNA–protein interference effect than MurNAc-6-P. To further investigate the regulatory mechanism and the substrate specificity of MurR, we crystallized and solved the structures of apo MurR and MurR in complex with MurNAc-6-P and GlcNAc-6-P. The specific contacts in MurR/MurNAc-6-P differ from that in MurR/GlcNAc-6-P, which explains the reason why MurNAc-6-P binds with a higher affinity than GlcNAc-6-P. The work presented here revealed the molecular mechanism of MurR-mediated cell-wall recycling in *E. coli* and might serve as a paradigm for other bacteria.

MATERIALS AND METHODS

Bacterial strains, plasmids and growth conditions

The bacterial strains and plasmids used in this study are listed in supporting information (SI), Supplementary Table S1. Primers used in this study are listed in SI, Supplementary Table S2. Unless otherwise specified, *E. coli* strains were grown in LB-Miller (simplified as LB) at 37°C. When necessary, antibiotics were used at the following concentrations: 50 μg/ml kanamycin and 50 μg/ml carbenicillin.

Construction of the plasmids and strains

The pKD46-Cas9-RecA-Cure/pCRISPR system (40) was used to construct the *murR*-deletion strain. Spacers of *murR* were inserted into pCRISPR plasmid, and the resulting plasmids were extracted using the SPARKeasy Superpure Mini Plasmid Kit (Sparkjade, Shandong, China). Then the pCRISPR-spacer plasmid and a 90-nt repair template were co-electroporated into the *E. coli* strains (MG1655 and BW25113) containing pKD46-Cas9-RecA-Cure. After verifying the deletion of *murR* via PCR using Taq DNA Polymerase (Sangon Biotech, Shanghai, China) and Sanger sequencing, the successfully mutated cells were subjected to cure the plasmids.

The lambda Red-recombineering method (41) was used to construct the complementary strain of *murR*-deletion mutant and the single-mutation strains. The pUC19-FRT-km-murR plasmid which contains the kanamycin resistance cassette from pKD4 and the *murR* gene from MG1655 genomic DNA were initially constructed. Then, the single mutations in the *murR* gene were introduced into the vector via site-directed mutagenesis. The repair templates were amplified from the pUC19-FRT-km-murR plasmids and were electroporated into the MG1655 strain containing pKD46. After verifying the insertion of *murR* by PCR and Sanger sequencing, the cells were subjected to cure the plasmid.

For protein expression, the WT *murR* gene was PCR-amplified from *Escherichia coli* MG1655 genomic DNA and cloned into the pET28a expression vector encoding a human rhinovirus 3C (HRV3C) protease cleavage site and an N-terminal His6-tag. The truncated *murR* genes (T1 and T2) for crystallization were cloned into the pET28a-HRV3C vector following the same process. Mutations of *murR* gene were then introduced into pET28a-HRV3C-*murR* via PCR-mediated site-directed mutagenesis.

To generate the MurR-dependent reporter vector, T7 promoter, ribosome binding site, the coding sequence of eGFP and the intergenic region between *murQ* and *murR* were ligated via Gibson Assembly. All of the plasmids and strains used in this study were verified via PCR and Sanger sequencing.

Synthesis of MurNAc-6-P

All commercial materials were used as received unless otherwise noted. Thin layer chromatography (TLC) was performed on silica gel F254 pre-coated glass plates (HSGF254, Huanghai) and visualized by irradiation under a 254 nm UV lamp or by treatment with a solution of phosphomolybdic acid in ethanol (5 wt%) followed by heating. Flash chromatography was performed using SepaFlash® silica flash column (Santai Technologies, Inc.). NMR spectra were recorded on Bruker AVANCE III HD 400 instruments and calibrated using tetramethylsilane (TMS) as internal reference. Multiplicities are recorded as: s = singlet, d = doublet, t = triplet, dd = doublet of doublets, m = multiplet, br = broad. ESI mass experiments were operated on Agilent 1260 Infinity/6120 Quadrupole LC/MS. Compound **2, 3, 4** was prepared according to the related references (42–44). The procedure for the synthesis of compound **5**, **6** and **7** (MurNAc-6-phosphate) was adapted from the literature methodology (30).

Benzyl 2-acetamido-4-*O*-benzyl-3-*O*-(D-1-carboxyethyl)-2-deoxy-α-D-glucopyranoside (5). Compound **4** (666 mg, 1.41 mmol) was dissolved in 50 ml of distilled CH_2Cl_2, and the solution was stirred for 1 h under an argon atmosphere in the presence of 4 Å molecular sieves at rt. The reaction mixture was cooled to −78°C, and triethylsilane was added (1.35 ml, 8.48 mmol). After 5 min, dichlorophenylborane (1.11 ml, 8.48 mmol) was added to the reaction mixture, and the stirring was continued at −78°C. The reaction progress was monitored for the disappearance of starting material by TLC analysis (5:1 CH_2Cl_2/MeOH mixture) and was judged to be complete after 2 h. The reaction was quenched at −78°C with 1.25 ml of NEt_3 and 1.25 ml of MeOH, and the mixture was allowed to warm to room temperature. The solution was diluted with 25 ml of CH_2Cl_2 and washed twice with 75 ml of cold H_2O and once with 50 ml of saturated NaCl. The aqueous washes were combined and acidified with concentrated HCl and subsequently extracted multiple times with CH_2Cl_2. All organic extracts were pooled and dried over $MgSO_4$ before being concentrated *in vacuo*. Silica gel chromatography (10:1 CH_2Cl_2/MeOH mixture and then 4:1 CH_2Cl_2/MeOH mixture) gave compound **5** as white solid (300 mg, 45%). ^{1}H NMR (400 MHz, MeOD) δ 7.36–7.24 (m, 10H), 5.12 (d, J = 1.6 Hz, 1H), 4.79–4.68 (m, 3H), 4.54–4.47 (m, 2H), 3.77–3.60 (m, 6H), 1.94 (s, 3H), 1.34 (d, J = 7.0 Hz, 3H); ^{13}C NMR (101 MHz, MeOD) δ 177.15, 171.95, 138.05, 137.60, 128.13, 127.99, 127.68, 127.50, 127.42, 95.72, 79.16, 77.44, 75.63, 74.62, 72.26, 69.05, 60.43, 54.34, 21.33, 18.30; ESI-MS m/z 472.1 $[M-H]^-$, m/z 474.3 $[M + H]^+$.

Benzyl 2-acetamido-4-*O*-benzyl-3-*O*-(D-1-carboxyethyl)-2-deoxy-6-*O*-dibenzylphosphoryl-α-D-glucopyranoside (6). To a solution of compound **5** (330 mg, 0.70 mmol) in 30 ml of distilled CH_2Cl_2 under an argon atmosphere was added triazole (193 mg, 2.80 mmol). To this mixture was added dibenzyl *N*,*N*- diisopropylphosphoramidite (604 mg, 1.75 mmol), and the reaction mixture was stirred at room temperature for 3 h. The reaction mixture was diluted with 120 ml of Et_2O and washed with 90 ml each of H_2O and saturated NaCl. The organic layer was dried over $MgSO_4$ and concentrated in vacuo to generate the crude phosphite sugar. The crude phosphite sugar residue was dissolved in 20 ml of THF and cooled to −78°C before 5 ml of 30% H_2O_2 was added. The reaction mixture was allowed to warm to room temperature, subsequently poured into 80 ml of Et_2O, and successively washed with 3 × 30 ml of ice-cold H_2O and 40 ml of saturated NaCl. The aqueous washes were pooled and acidified with concentrated HCl and extracted with CH_2Cl_2. The combined organic extracts were dried over $MgSO_4$ and concentrated *in vacuo*. Silica gel chromatography (CH_2Cl_2, then 9:1 CH_2Cl_2/MeOH mixture, and then 4:1 CH_2Cl_2/MeOH mixture) afforded compound **6** as white foam (170 mg, 33%): ^{1}H NMR (400 MHz, MeOD) δ 7.41–7.21 (m, 20H), 5.12–5.01 (m, 5H), 4.72–4.54 (m, 3H), 4.53–4.40 (m, 2H), 4.17–4.09 (m, 2H), 3.78–3.70 (m, 3H), 3.52–3.43 (m, 1H), 1.94 (s, 3H), 1.35 (d, J = 6.9 Hz, 3H); ^{13}C NMR (101 MHz, MeOD) δ 178.32, 171.98, 137.71, 137.41, 135.75 (d, J = 6.6 Hz), 128.36, 128.33, 128.15, 128.01, 127.76, 127.73, 127.71, 127.56, 127.48, 127.45, 95.81, 78.73, 77.26, 74.68, 70.21 (d, J = 7.5 Hz), 69.52, 69.52 (d, J = 12.6 Hz), 69.41, 66.28 (d, J = 5.8 Hz), 54.19, 21.29, 18.29; ^{31}P NMR (162 MHz, MeOD) δ −1.33; ESI-MS m/z 732.3 $[M-H]^-$, m/z 734.3 $[M + H]^+$.

2-Acetamido-3-*O*-(D-1-carboxyethyl)-2-deoxy-α,β-D-glucose 6-dihydrogen phosphate (7, MurNAc-6-P). Compound **6** (170 mg, 0.23 mmol) was hydrogenated (50 psi) over $Pd(OH)_2$ (10 wt.% on activated carbon, 17 mg, 0.012 mmol, 5 mol%) in distilled MeOH (30 ml) with a catalytic amount of acetic acid (25 μl) at 60 °C for 48 h. The reaction was judged to be completed by LC–MS analysis, and the mixture was filtered through a pad of Celite and the filtrate concentrated *in vacuo*. The residue was dissolved in a minimal amount of MeOH, toluene added, and the mixture concentrated to remove any residual amounts of acetic acid. The residue was dissolved in H_2O and loaded onto a 10 ml column of AG-1 × 8 resin (formate form). The column was washed with 50 ml each of H_2O and 1.4, 2.8, 4.2 and 5.6 N formic acid, and each of the fractions was analyzed by LC–MS for the presence of MurNAc-6-phosphate. Fractions found to contain product (collected between 4.2 and 5.6 N formic acid) were pooled, and the volume was reduced on a rotary evaporator. Distilled H_2O was added and the remaining solvent evaporated; this procedure was repeated multiple times to remove any remaining formic acid and gave 45 mg (53%) of MurNAc-6-phosphate. The phosphate sugar was dissolved in 10 ml of H_2O and carefully titrated to pH 7.5 with NaOH. The resulting solution was frozen and lyophilized to give the disodium salt of MurNAc-6-phosphate as a white solid. α-Anomer: ^{1}H NMR (400 MHz, D_2O) δ 5.47 (d, J = 3.0 Hz, 1H), 4.40 (q, J = 6.9 Hz, 1H), 3.99–3.77 (m, 3H), 3.70–3.40 (m, 3H), 1.97 (s, 3H), 1.29 (d, J = 7.0 Hz, 3H); β-Anomer: ^{1}H NMR (400 MHz, D_2O) δ 4.60 (d, J = 8.2 Hz, 1H), 4.24 (d, J = 7.0 Hz, 1H), 3.99–3.77 (m, 3H), 3.70 – 3.40 (m, 3H), 1.97 (s, 3H), 1.25 (d, J = 6.6 Hz, 3H); ^{31}P NMR (162 MHz, D_2O) δ 4.33; ESI-MS m/z 372.1 $[M-H]^-$.

Protein expression and purification

The expression plasmids were transformed into *E. coli* BL21 (DE3), and then the cells were grown in LB supplemented with 0.5 mM IPTG when OD_{600} reached to 0.6. The induced cells were further cultured overnight at 16°C and harvested by centrifugation at 6000 g for 10 min. Cell pellets were resuspended in the lysate buffer (500 mM NaCl, 10 mM Tris·HCl pH 7.5, 5% glycerol, 1 mM DTT), and disrupted by sonication. The supernatant was then loaded onto a His-Trap HP column (GE Healthcare). The column was orderly washed with the lysate buffer containing 62.5 mM imidazole, and the desired protein was eluted with the lysate buffer containing 500 mM imidazole. To remove the 6XHis tag, the eluted proteins were processed by the HRV3C protease at 4°C overnight and then clarified with the His-Trap HP column. The processed proteins were further purified by using a HiLoad 16/600 Superdex 200 pg column (GE Healthcare) in the elution buffer (100 mM NaCl, 10 mM Tris·HCl pH 7.5, 1 mM DTT). The eluted proteins were concentrated for further utilization.

Analytical size-exclusion chromatography

To investigate whether the signaling molecule could change the multimerization state of MurR, 200 μM WT MurR and the mutant MurR proteins were separately incubated with 1 mM MurNAc-6-P in the reaction buffer (100 mM NaCl, 10 mM Tris·HCl pH 7.5, 1 mM DTT) at room temperature for 10 min. Then, the samples were analyzed by a 25 ml Superose 6 10/300 GL column (GE Healthcare).

Analytical ultracentrifugation

Sedimentation velocity experiments were performed on the Beckman ProteomeLab™ XL-I analytical ultracentrifuge. The full-length MurR protein was purified by using a HiLoad 16/600 Superdex 200 pg column (GE Healthcare) in the elution buffer (100 mM NaCl, 10 mM Tris·HCl pH 7.5, 1 mM DTT) and then diluted to 20 μM for sedimentation velocity experiments under 42000 rpm at 10°C. Partial specific volume of MurR, buffer density and buffer viscosity were calculated using the SEDNTERP software. The sedimentation velocity data were analyzed and fitted to a continuous sedimentation coefficient distribution model using the SEDFIT software. The $c(s)$ distribution was further transformed from the experimental s to the standardized $s_{20,w}$ using the GUSSI software.

Protein crystallization

The apo MurRT1 (S94 to N266) protein, MurRT2 (D95 to K285)/MurNAc-6-P and MurRT2/GlcNAc-6-P complexes were crystallized by using the sitting-drop vapor-diffusion method at 16 °C. MurNAc-6-P was chemically

synthesized and characterized (Supplementary Figures S1 and S2). GlcNAc-6-P was purchased from J&K Scientific Chemical Inc (Shanghai, China). To obtain the apo MurRT1 crystals, 1 μl protein solution (10 mg/ml in 100 mM NaCl, 10 mM Tris–HCl pH 7.5, 1 mM DTT) was mixed with 1 μl reservoir solution containing 0.2 M L-proline, 0.1 M HEPES pH 7.5, 10% (w/v) polyethylene glycol 3350. For co-crystallization, MurRT2 was incubated with MurNAc-6-P in a 1:5 molar ratio on ice for 30 min, and then mixed with the reservoir solution containing 0.02 M citric acid, 0.08 M Bis–Tris propane pH 8.8, 16% (w/v) polyethylene glycol 3350. For crystallization of MurRT2/GlcNAc-6-P complex, MurRT2 was incubated with GlcNAc-6-P in a 1:50 molar ratio on ice for 30 min, and then mixed with the reservoir solution containing 20% (v/v) 2-propanol, 0.1 M Tris pH 8.0, 5% (w/v) polyethylene glycol 8000. The crystals were cryo-protected and stored in liquid N_2 before data collection.

Data collection, structure determination and refinement

The data were collected at BL19U1 beamline of National Facility for Protein Science Shanghai (NFPS) at Shanghai Synchrotron Radiation Facility. The data were processed by HKL3000. The phase of apo MurR was determined by Phaser from CCP4i suits using the structure of *Vibrio vulnificus* NanR (PDB ID: 4IVN) as the search model. The phases of the MurR/MurNAc-6-P and MurR/GlcNAc-6-P complexes were determined by Phaser using the structure of apo MurR as the search model. The models were built by Autobuild from PHENIX suits. The models of apo MurR, MurR/MurNAc-6-P and MurR/GlcNAc-6-P were refined using Refmac5 of ccp4i suits. These refined models were further manually improved by coot. Structural figures were prepared using PyMOL (http://www.pymol.org).

Isothermal titration calorimetry (ITC)

The association constants were measured via the MicroCal ITC200 system (Malvern, UK). Proteins and ligands were diluted to 50 μM and 500 μM, respectively, using the same buffer containing 100 mM NaCl, 10 mM Tris–HCl, pH 7.5, 1 mM DTT. The ligands in the syringe were slowly titrated into the reaction cell containing protein solutions. The assay was performed at 25 °C with a stirring speed of 750 rpm and held 120 s between two injections. Raw data were processed and plotted by using the Origin7 software package (Malvern, UK). All data are background-subtracted. All the experiments were performed in triplicate.

Electrophoretic mobility shift assay (EMSA)

DNA fragment containing the *murR-murQ* intergenic region was amplified with the FAM-labeled primers from the MG1655 genome and then gel purified. The control DNA fragment was amplified with the FAM-labeled primers from the *Pseudomonas aeruginosa* PAO1 genome and then gel purified. The DNA fragment (10 nM) was incubated with different concentrations of protein in the presence or absence of MurNAc-6-P/GlcNAc-6-P in the reaction buffer (100 mM NaCl, 10 mM Tris·HCl pH 7.5, 1 mM DTT). The mixtures were incubated for 10 min at room temperature and then mixed with 5 μl of the same buffer supplemented with 40% (v/v) glycerol and bromophenol blue. Free DNA and MurR–DNA complexes were separated on 6% polyacrylamide gels in TB buffer (54 g/l Tris base, 27.5 g/l boric acid). Results were visualized by the Gel Imager System (Bio-Rad, USA).

Fluorescent quantitation assay

To explore the binding capacity of MurR proteins to the target DNA, the plasmids (5.8 nM) were mixed with different concentrations of proteins in the CFPS system. For the investigation of the influence of MurNAc-6-P/GlcNAc-6-P to the MurR-DNA complexes, the plasmids (5.8 nM) were mixed with the protein in a 1:100 molar ratio with different concentrations of MurNAc-6-P/GlcNAc-6-P. Fluorescence of the eGFP was monitored by the CFX96™ Real-Time System (Bio-Rad, USA). All the experiments were performed in triplicate.

mRNA transcription level measurement

E. coli BW25113 strains were cultured to the stationary phase in LB medium. Then the total RNAs were extracted using the MiniBEST Universal RNA Extraction Kit (Takara, Japan), and then were used as templates for reverse transcription with the TransScript® One-Step gDNA Removal and cDNA Synthesis SuperMix (TransGen Biotech, Beijing, China). The qPCR reaction was carried out using the ChamQ Universal SYBR qPCR Master Mix (Vazyme Biotech, Nanjing, China). The fluorescence of the amplified DNA was monitored by the LightCycler®96 Real-Time System (Roche, Switzerland). The *rpsL* gene of *E. coli* was used as the reference gene. All the experiments were performed in triplicate.

Growth curve assays

The growth of *E. coli* MG1655 strains were monitored via the automated microbe growth curve analysis system Bioscreen C (OY Growth Curves Ltd, Finland). Overnight cultures incubated in 3 ml MMA-0.2% GlcNAc were washed twice and resuspended using MMA (29), and then 1:100 diluted into 200 ul MMA-0.2% MurNAc/GlcNAc. The plates were continuously shooked at 37°C and measured every 1 h. All the experiments were performed in triplicate.

RESULTS

MurR discriminatively interacts with MurNAc-6-P and GlcNAc-6-P

Gene neighborhood and phylogenetic analysis (45) revealed that MurR/MurR-like regulators are conserved in a number of Gram-negative and Gram-positive bacterial species, such as *Escherichia coli*, *Shigella dysenteriae*, *Citrobacter koseri*, *Staphylococcus aureus*, *Bacillus subtilis* and *Streptomyces coelicolor* (Supplementary Figure S3 and Supplementary Table S3). Previous studies have demonstrated that the deletion of *murR* markedly increased the expression of MurP and MurQ, causing more efficient transportation and

metabolism of MurNAc, thus making *E. coli* grow faster in logarithmic phase when MurNAc is used as the sole carbon source (39). To verify this conclusion, we measured the mRNA transcription levels of *murQ*, *murP* and *pbp4B*, another gene controlled by MurR. As shown in Supplementary Figure S4, the deletion of *murR* evidently increased the transcription levels of all three genes. Then, we cultivated the wild-type (WT) *E. coli* K-12 strain MG1655 and the *murR*-deletion mutant in minimal medium A (29) (MMA) supplemented with 0.2% (wt/vol) MurNAc. As shown in Figure 2A, WT strain exhibited a slower growth rate than the *murR* deletion mutant, suggesting that MurR might play an important role when *E. coli* cells grow in a nutrient-deficient environment. However, when these two strains were grown in MMA medium supplemented with another saccharide GlcNAc, no visible difference was observed (Figure 2B). This result indicated that the pathway regulated by MurR showed substrate specificity toward different saccharides.

To further investigate the interaction between MurR and its known signal molecule, MurNAc-6-P, we employed isothermal titration calorimetry (ITC) to examine the binding affinity between MurR and MurNAc-6-P. The titration of MurR with MurNAc-6-P released a significant amount of heat with a dissociation constant (K_d) of 4.3 μM and stoichiometry of nearly 1:1 (Figure 2C), indicating that one molecule of MurNAc-6-P binds to one MurR molecule with a strong protein–ligand interaction. We also measured the binding affinity between MurR and different intermediates of amino sugar metabolism. Intriguingly, when we titrated MurR with GlcNAc-6-P, the product metabolized by the etherase MurQ from MurNAc-6-P, an obvious interaction was detected with a measured K_d value of 17.6 μM and stoichiometry of nearly 1:1 (Figure 2D), while no interaction was observed when titrating MurNAc and GlcNAc into MurR (Supplementary Figure S5 A and B). Therefore, we suspected that GlcNAc-6-P might be another signaling molecule for MurR.

MurR represses the transcription of *murQP* and *murR* by binding separately to each operator within the *murR-murQ* intergenic region (39) (Supplementary Figure S6). To examine the binding ability of MurR with its operator DNA, we performed an electrophoretic gel mobility shift assay (EMSA), in which the FAM-labeled DNA fragments harboring the *murR-murQ* intergenic region were incubated with an increasing amount of MurR. As shown in Figure 2E and Supplementary Figure S7 A, MurR effectively bound to the promoter DNA, and a concentration of 160 nM MurR shifted most of the DNA. To further investigate the effects of MurNAc-6-P and GlcNAc-6-P on MurR-DNA binding, 200 nM MurR was incubated with the promoter DNA in the absence or presence of increasing amounts of MurNAc-6-P and GlcNAc-6-P, respectively. As shown in Figure 2F, Supplementary Figure S7B, Supplementary Figure S8 A and B, the addition of MurNAc-6-P obviously relieved the retardation of DNA migration and half of the MurR/DNA complex was dissociated when the concentration of MurNAc-6-P reached approximately 400 μM, indicating that MurNAc-6-P is adverse to the binding of MurR with DNA. Interestingly, we found that MurR protein tended to aggregate at a high concentration of MurNAc-6-P for unknown reasons (Figure 2F and Supplementary Figure S8A). The EMSA revealed the competitive effect that MurNAc-6-P disrupts the binding of MurR with the promoter DNA. In contrast, the relief of the retardation was negligible when the same concentration of GlcNAc-6-P was added (Figure 2F, Supplementary Figure S7B). We observed that a certain portion of the DNA was dissociated from MurR when the concentration of GlcNAc-6-P increased to 40 mM (Figure 2G). To clarify that the DNA shift was not caused by the ionic strength of GlcNAc-6-P, the same concentrations of sodium sulfate were added into the same reaction solution, and the binding of MurR with DNA was not affected (Figure 2G). The EMSA reveals the distinctly competitive effect that MurNAc-6-P disrupts the binding of MurR and the promoter DNA, which probably requires higher concentrations of ligands than the K_d value measured by ITC. These results indicated that both MurNAc-6-P and GlcNAc-6-P could alleviate the interaction between MurR and its operator DNA, but the influence of GlcNAc-6-P in MurR DNA binding is significantly weaker than that of MurNAc-6-P, which is probably due to the relatively lower binding affinity between GlcNAc-6-P and MurR.

Structural characterizations of apo MurR, MurR/MurNAc-6-P and MurR/GlcNAc-6-P

To elucidate the molecular mechanism of how MurR interacts with its signaling molecules, we sought to determine its crystal structures. The size-exclusion chromatography analysis and the sedimentation velocity analysis of full-length MurR unveiled that MurR forms a tetramer (125 KDa) rather than a dimer (62 KDa) in solution, which is consistent with previous findings (39) (Supplementary Figure S9). Structural prediction revealed that MurR consists of two major functional domains, the HTH DNA binding domain (M1-S77) and the SIS ligand binding domain (I128-V268) (Figure 3A). After trying different truncated proteins and screening hundreds of crystallization conditions for each truncation, truncated protein 1 (named MurRT1, containing the amino acids from S94 to N266), harboring the whole ligand-binding domain (LBD), was eventually crystallized with the space group $P2_12_12_1$ and a resolution of 2.27 Å (Supplementary Table S4). Apo MurR contains four monomers in an asymmetric unit (Figure 3B), possibly indicating the functional tetrameric form of MurR in cells. Each MurRT1 protein forms an α/β-fold structure containing five parallel β-sheets and seven α-helices, whereas the α-helices in the C-terminal are omitted due to the poor electron density (Supplementary Figure S10). In addition, crystals of MurR/MurNAc-6-P and MurR/GlcNAc-6-P complexes were also successfully obtained when another truncated protein (named MurRT2, harboring the amino acids from D95 to K285) was used. The two complexes were both crystallized in the space group *I222*, and the structures were refined to resolutions of 1.22 Å (MurR/MurNAc-6-P) and 1.25 Å (MurR/GlcNAc-6-P) (Supplementary Table S4). Both the asymmetric units of MurR/MurNAc-6-P and MurR/GlcNAc-6-P complexes contain one monomer (Supplementary Table S4), and the overall structures of MurR/MurNAc-6-P and MurR/GlcNAc-6-P are shown

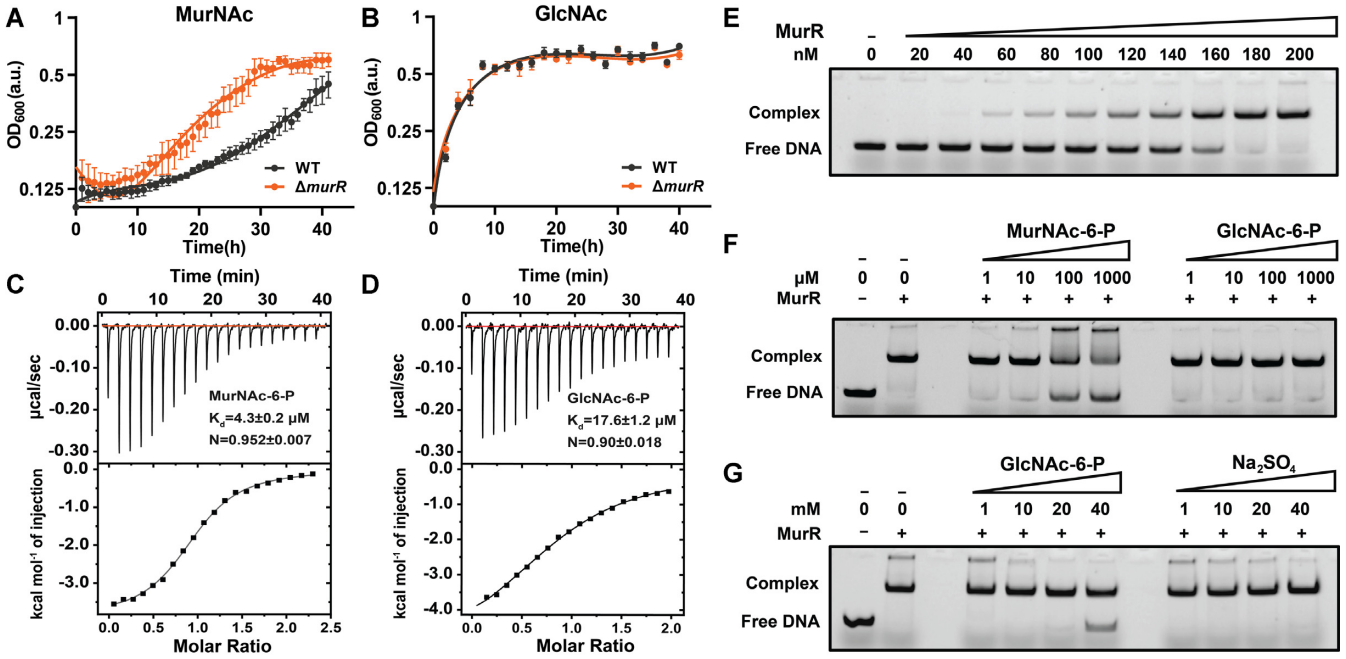

Figure 2. Assessment of the effect of MurNAc-6-P and GlcNAc-6-P on MurR. (A and B) Growth curve of *E. coli* MG1655-WT strain and MG1655-Δ*murR* mutant in MMA medium supplemented with 0.2% (wt/vol) MurNAc (**A**) and GlcNAc (**B**). The OD_{600} is in arbitrary unit (a.u.). Data represent the mean ± s.d. of three biological replicates. (C and D) ITC assay for the binding between MurR and MurNAc-6-P (**C**), and GlcNAc-6-P (**D**). K_d, the dissociation constant; *N*, the number of binding sites per MurR. (E–G) EMSA analysis of the interaction between MurR and its operator DNA in the absence (**E**) or presence of 1, 10, 100, 1000 μM MurNAc-6-P or GlcNAc-6-P (**F**), 1, 10, 20, 40 mM GlcNAc-6-P or Na_2SO_4 (**G**).

in the tetrameric forms (Figure 3C and D). Each monomer in both complex structures contains five parallel β-sheets and 8 α-helices (Figure 3E and F) and a well-defined saccharide molecule (Figure 3C and D) that resides in the central pocket (Supplementary Figure S11 A and B). The structures of MurR/GlcNAc-6-P and MurR/MurNAc-6-P possess almost identical overall conformations with a 0.133-Å root-mean-square deviation (rmsd), which is calculated by overlaying the skeletal atoms of the main-chain of each monomer automatically excluding 26 residues (D95/R124/G144/G145/A165/C166/E167/A168/D169/V172/K182/G183/Q264/I265/I274/Q275/R276/S277/S278/E279/I280/T281/Q282/R283/I284/K285) (Figure 3G). In addition, we observed a conformational rearrangement in the ligand-binding pocket after ligand association with MurR (Supplementary Figure S11A–C).

Detailed interactions between MurR and saccharide molecules

A close view of the ligand-binding pockets of the MurR/MurNAc-6-P complex revealed extensive interactions between MurR and MurNAc-6-P, including direct hydrogen bonds (≤3.2 Å), water-mediated hydrogen bonds (≤3.2 Å) and van der Waals contacts (≤4.0 Å). In total, 8 residues (G145, S146, K159, H171, S190, Y191, S192 and K195) directly engage in contacts with MurNAc-6-P, 3 residues (L143, I189 and T281) engage in water-mediated contacts, and 6 residues (L143, H171, T175, S244, S277 and T281) contact MurNAc-6-P via van der Waals contacts (Figure 4A and B, Supplementary Table S5). In the MurR/GlcNAc-6-P complex, the direct hydrogen bond between G145 and GlcNAc-6-P becomes weaker, and K159 forms a water-mediated hydrogen bond with GlcNAc-6-P instead of a direct hydrogen bond in the MurR/MurNAc-6-P structure. In addition, H171 forms another water-mediated hydrogen bond with GlcNAc-6-P and a van der Waals contact via S244 in the MurR/MurNAc-6-P structure disappears in the MurR/GlcNAc-6-P structure (Figure 4C and D, Supplementary Table S5).

Three subunits of MurR contact each MurNAc-6-P or GlcNAc-6-P. In detail, MurNAc-6-P binds to MurR via the sites formed by α3 helix (G145, S146), α7 helix (S244), β3 sheet (I189, S190), L4 loop (L143), L8 loop (Y191, S192, K195) of monomer A, α3 helix (K159), α8 helix (S277, T281) of monomer B and α4 helix (H171, T175) of monomer C. The main-chain amide of Y191, S192 and side-chain hydroxyl groups of three serine residues (S146, S190 and S192) play a primary role in the recognition of the phosphate group of MurNAc-6-P. The backbone amides of G145 and Y191 form a direct hydrogen bond with the hydroxyl oxygen atom of C4 of MurNAc-6-P, while the side-chain amine of K159 forms a direct hydrogen bond with the carboxyl oxygen atom of the lactic group. The hydroxyl group in position C1 of MurNAc-6-P coincidently forms hydrogen bonds with the side-chain imidazole nitrogen atom of H171 and the side-chain amine of K195. In addition, three residues (L143, I189 and T281) provide three additional water-mediated hydrogen bonds with MurNAc-6-P. Moreover, 4 carbon atoms of 2 residues (L143 and H171) contact the carbon atoms of the anhydride ring, 7 carbon atoms of 5 residues (L143, T175, S244, S277 and T281) contact the side-chain carbon atoms of MurNAc-6-P through van der Waals interactions.

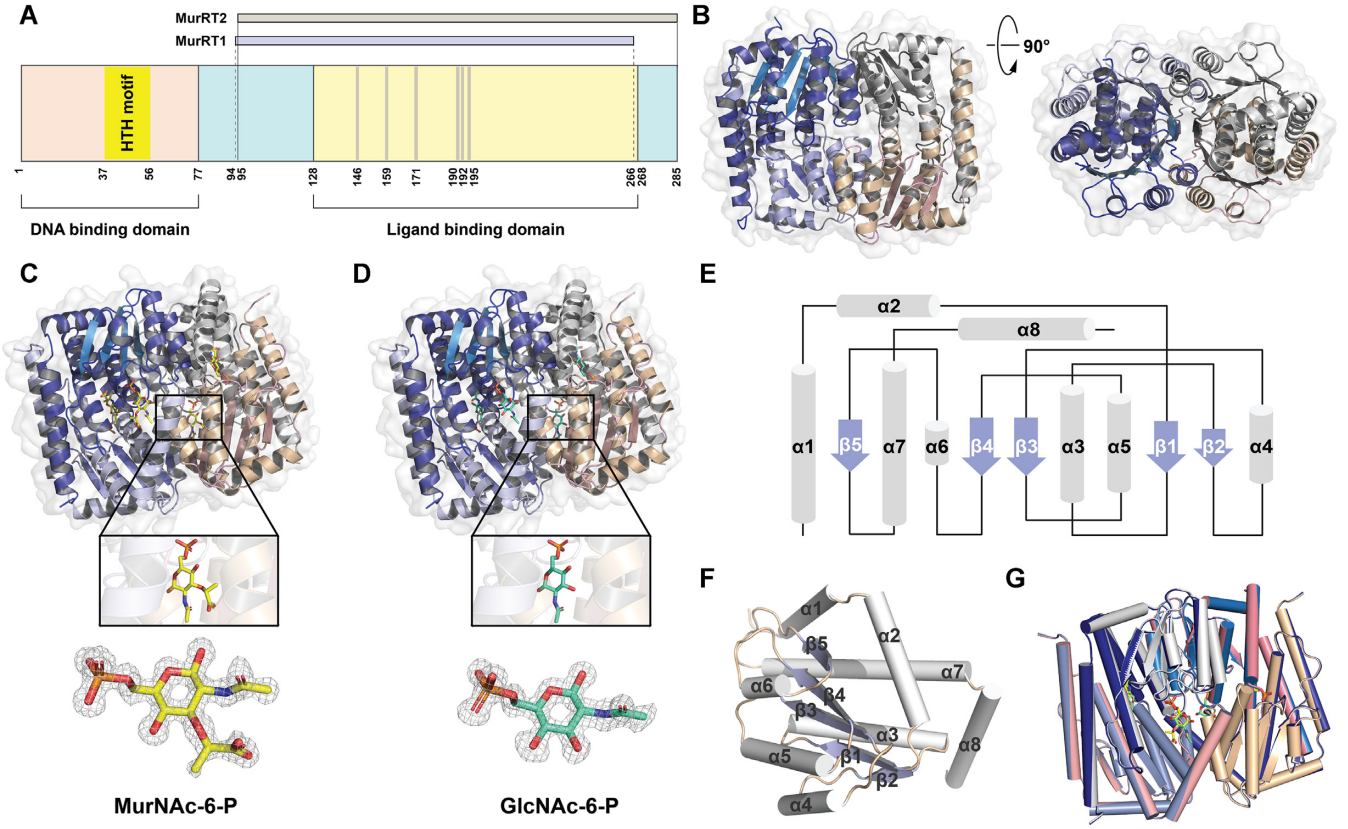

Figure 3. Structural characterizations of apo MurR, MurR/MurNAc-6-P and MurR/GlcNAc-6-P. (**A**) The domain organization of full-length MurR. (**B**) The overall structure of apo MurR. (**C**) The overall structure of MurR/MurNAc-6-P and the detailed view of the electron density of MurNAc-6-P. 2*Fo* – *Fc* map (1.0 σ) is shown as a gray mesh. (**D**) The overall structure of MurR/GlcNAc-6-P and the detailed view of the electron density of GlcNAc-6-P. 2*Fo* – *Fc* map (1.0 σ) is shown as a gray mesh. (**E**) Schematic representation of the topology of MurR. (**F**) Cartoon of MurR in its monomeric form. α-helices, β-sheets are colored in grey and lightblue, respectively. (**G**) Structure overlay of MurR/MurNAc-6-P and MurR/GlcNAc-6-P. The monomers of MurR/MurNAc-6-P are colored gray, boron, wheat and cobalt, respectively. The monomers of MurR/GlcNAc-6-P are colored blue, chromium, deepblue and rhenium, respectively.

Analogously, GlcNAc-6-P interacted with MurR via the α3 helix (S146), β3 sheet (I189, S190), L4 loop (L143), L8 loop (Y191, S192, K195) of monomer A, α3 helix (K159), α8 helix (S277, T281) of monomer B and α4 helix (H171, T175) of monomer C. In contrast, the backbone amide of G145 forms a weaker interaction with the hydroxyl oxygen atom of C4 of GlcNAc-6-P. Due to the lack of a lactic group in GlcNAc-6-P, K159 could not form a direct hydrogen bond with the carboxyl oxygen atom, and instead, the side-chain amine of K159 forms a water-mediated hydrogen bond with the hydroxyl oxygen atom of C3 of GlcNAc-6-P. The side-chain carbon atom of S244 lacks a van der Waals interaction with GlcNAc-6-P for the same reason. Moreover, the backbone carboxyl of H171 contacts the acetyl nitrogen atom of GlcNAc-6-P via water-mediated hydrogen bonds.

Interestingly, superimposition of the ligand-binding pockets of MurR/MurNAc-6-P and MurR/GlcNAc-6-P revealed that some interactions between MurR and the ligands were changed (Figure 4E). One direct hydrogen bond between G145 and the hydroxyl oxygen atom of C5 of GlcNAc-6-P becomes weaker compared with that in the MurR/MurNAc-6-P structure. The direct hydrogen bond between K159 and the lactic group of MurNAc-6-P is replaced by a water-mediated hydrogen bond formed by K159 and the hydroxyl oxygen atom of C3 of GlcNAc-6-P, while the water-mediated hydrogen bond between MurR (H171) and GlcNAc-6-P is stronger than that between MurR and MurNAc-6-P. Meanwhile, four van der Waals interactions between MurR (L143, H171, S244, T281) and MurNAc-6-P showed a tighter interaction than that in the MurR/GlcNAc-6-P structure. Together, interactions between MurR and MurNAc-6-P seem to be more close-knit than those between MurR and GlcNAc-6-P, which are likely caused by the lactic group. Due to the lack of the lactic group in GlcNAc-6-P, K159 forms a water-mediated hydrogen bond with GlcNAc-6-P. In contrast, MurNAc-6-P possesses a lactic acid moiety that directly interacts with K159 via two direct hydrogen bonds, therefore having a higher binding affinity with MurR. Moreover, the lactic group of MurNAc-6-P forms a van der Waals contact with S244.

The interaction between MurNAc-6-P and MurR is vital for transcriptional regulation and growth

The detailed structural analysis revealed multiple interactions between MurR and MurNAc-6-P. To further verify the critical roles of these residues, the single amino acid

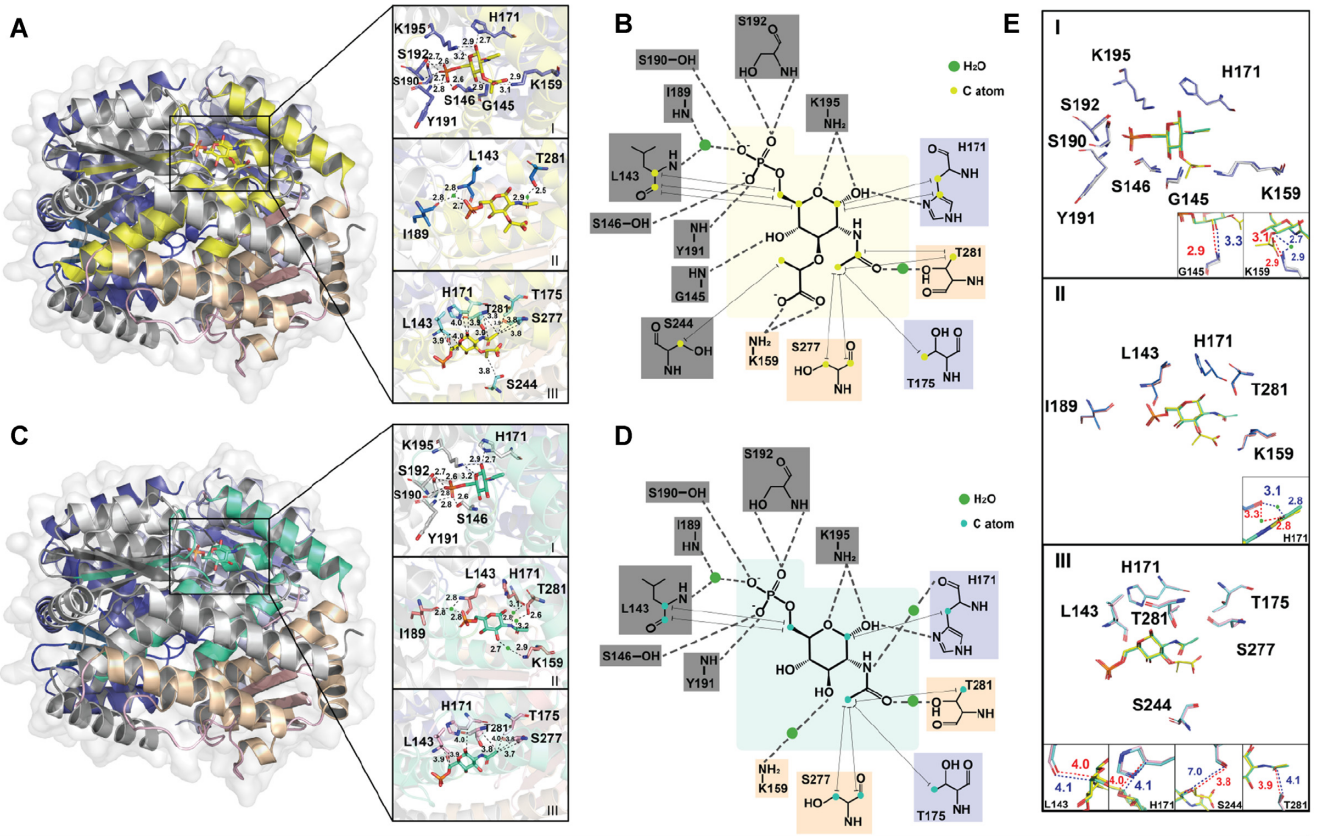

Figure 4. Detailed structural analysis of MurR/MurNAc-6-P and MurR/GlcNAc-6-P. (**A** and **B**) The detailed interactions between MurR and MurNAc-6-P. I, direct hydrogen bonds; II, water-mediated hydrogen bonds; III, van der Waals contacts. Chains are colored gray, wheat, bluewhite and deepblue, respectively. Yellow-colored spaces refer to structures interacted with MurNAc-6-P. Lines between two yellow balls refer to van der Waals contacts between MurR and MurNAc-6-P. (**C** and **D**) The detailed interactions between MurR and GlcNAc-6-P. I, direct hydrogen bonds; II, water-mediated hydrogen bonds; III, van der Waals contacts. Chains are colored gray, wheat, bluewhite and deepblue, respectively. Greencyan-colored spaces refer to structures interacted with GlcNAc-6-P. Lines between two greencyan balls refer to van der Waals contacts between MurR and GlcNAc-6-P. (**E**) Alignments of the key residues interacting with MurNAc-6-P/GlcNAc-6-P. I, direct hydrogen bonds; II, water-mediated hydrogen bonds; III, van der Waals contacts.

mutations S146A, K159A, H171A, S190A, S192A and K195A as well as the triple amino acid mutations KHK (K159A, H171A and K195A) and SSS (S146A, S190A and S192A) were separately introduced into the full-length MurR protein. As analyzed via size-exclusion chromatography and sodium dodecyl sulfate–polyacrylamide gel electrophoresis (SDS–PAGE), all of the mutant proteins shared approximately the same elution peak and showed similar purity, confirming that the single amino acid mutation did not affect protein expression and stability (Supplementary Figure S12 A and B). To further clarify the repressing/derepressing mechanism of MurR, we performed size-exclusion chromatography of WT MurR and mutated MurR proteins in the absence and presence of MurNAc-6-P, respectively. The elution peaks of MurR proteins are almost the same as those of the MurR/MurNAc-6-P complexes, demonstrating that the signal molecule does not change the multimerization state of MurR (Supplementary Figure S12C). Then we systematically examined the activity of the mutant proteins by ITC. The binding affinities between MurNAc-6-P and the mutant proteins S146A, H171A, S192A and K195A were dramatically decreased compared with those between WT MurR and MurNAc-6-P, and no detectable binding was observed when MurNAc-6-P was titrated into the K159A and S190A mutant proteins (Figure 5A, Supplementary Figure S13 A-F). The binding affinities between GlcNAc-6-P and these mutant proteins were also measured. Smaller association constant (K_a) values between these mutant proteins and GlcNAc-6-P were detected (Supplementary Figure S14A and B). Interestingly, when the alanine mutation was introduced into K159, which forms a direct hydrogen bond with MurNAc-6-P but interacts with GlcNAc-6-P through a water-mediated hydrogen bond, the mutant protein showed a similar binding affinity with GlcNAc-6-P compared with that of WT MurR, indicating that this residue is essential for MurNAc-6-P recognition but not for GlcNAc-6-P (Supplementary Figure S14C).

To assess the roles of these residues in MurNAc-6-P-mediated DNA dissociation, we performed EMSA in which the promoter DNA was incubated with the eight mutant proteins in the presence or absence of MurNAc-6-P. The DNA binding ability of the eight mutants was almost the same as that of the WT protein (Supplementary Figure S15 A and B). Compared with the WT protein whose binding affinity with DNA obviously decreased in the presence of

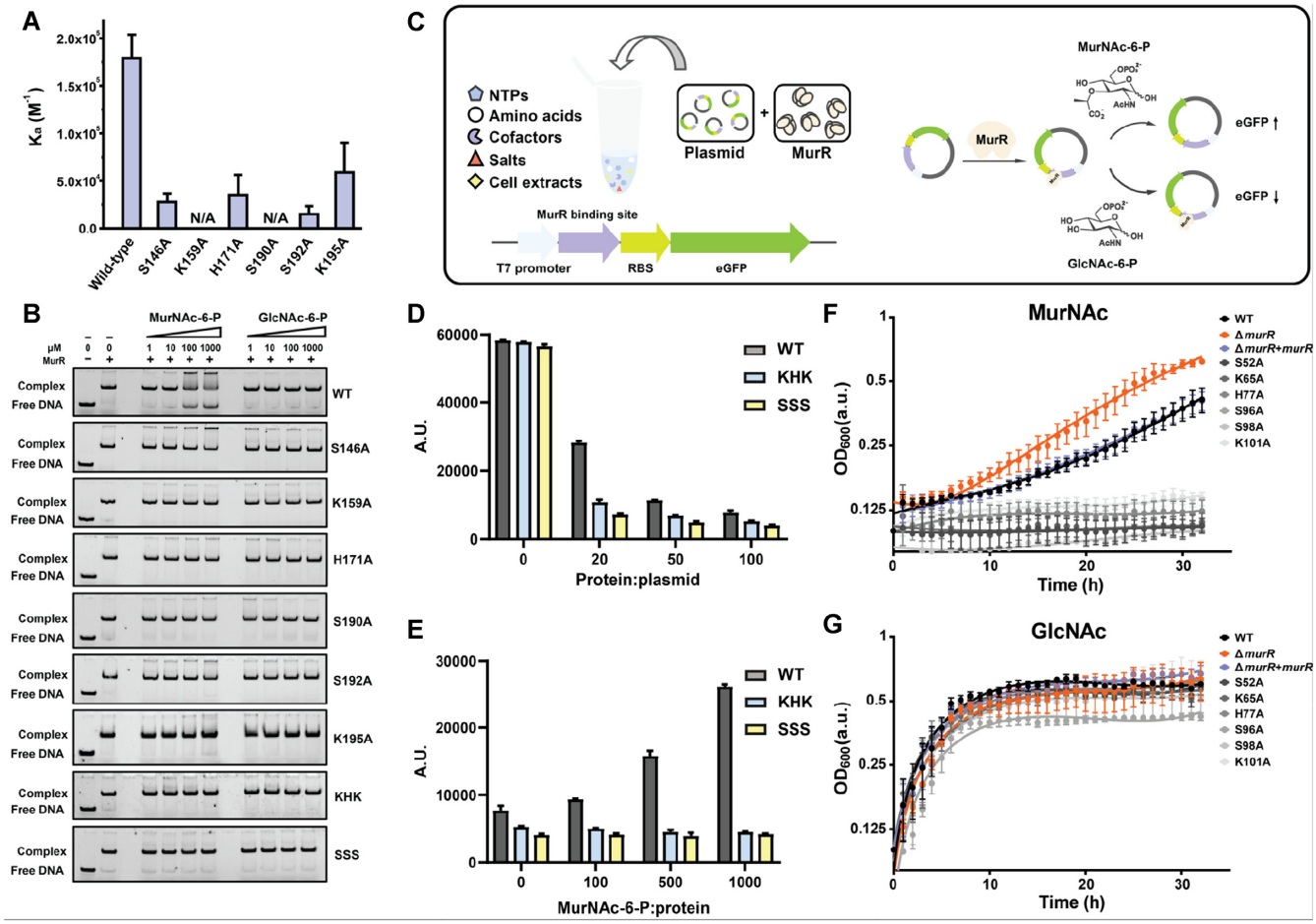

Figure 5. MurNAc-6-P recognition by MurR is vital for the regulation activity. (**A**) ITC assay for the binding between MurNAc-6-P and different mutant MurR proteins. Ka, the association constant; N/A, not available. Data represent the mean ± s.d. of three biological replicates. (**B**) EMSA analysis of the interaction between DNA fragment carrying the *murR-murQ* intergenic region and different mutant MurR proteins in the absence or presence of increasing amounts of MurNAc-6-P or GlcNAc-6-P. The gel electrophoresis image of WT protein is from Figure 2F. (**C**) The schematic diagram of the CFPS system. (D and E) The fluorescence values of the eGFP measured in the presence of different protein concentrations (**D**) and in the presence of different MurNAc-6-P concentrations (**E**). Data represent the mean ± s.d. of three biological replicates. (**F** and **G**) Growth curves of *E. coli* MG1655-WT, *murR*-deletion, complementary, S146A, K159A, H171A, S190A, S192A and K195A mutant strains in the presence of 0.2% (wt/vol) MurNAc (**F**) and GlcNAc (**G**). The OD_{600} is in arbitrary unit (a.u.). Data represent the mean ± s.d. of three biological replicates.

MurNAc-6-P, almost all of the mutant proteins were unresponsive to MurNAc-6-P treatment, releasing little free DNA from the protein/DNA complexes under the tested conditions (Figure 5B). Moreover, all of the MurR proteins were insensitive to GlcNAc-6-P at the tested concentrations (Figure 5B). These results demonstrated that the mutations of ligand-binding residues destroyed the interaction between MurR and MurNAc-6-P, and therefore the DNA binding activity of the mutant MurR proteins was not affected by MurNAc-6-P.

To visually assess the effect of MurNAc-6-P on MurR-mediated gene regulation *in vitro*, we employed the cell-free protein synthesis (CFPS) system (46,47), in which the expression of the enhanced green fluorescent protein (eGFP) was designed to be controlled by MurR, and thus the regulation capacity of MurR could be evaluated directly by the fluorescence intensity of eGFP. The CFPS system is composed of nucleoside triphosphates (NTPs), amino acids, cofactors, salts, and cell extracts, which are sufficient for protein expression (Figure 5C). We designed a vector pUC19-eGFP that contains the T7 promoter, ribosome binding site (RBS) and the coding sequence of eGFP. To investigate the regulatory mechanism of MurR, we constructed the pUC19-murR-eGFP plasmid by inserting the *murR-murQ* intergenic region between the T7 promoter and the RBS in pUC19-eGFP, which enabled MurR to regulate the expression of eGFP (Supplementary Figure S16). As shown in Figure 5D and Supplementary Figure S17A, strong eGFP fluorescence was detected when the plasmids were introduced into the CFPS system, indicating that the eGFP could be efficiently expressed. The fluorescence intensity of pUC19-murR-eGFP gradually decreased with increasing concentrations of MurR protein, whereas the fluorescence intensity of pUC19-eGFP remained constant. This result demonstrated that MurR could efficiently and specifically regulate the expression of eGFP. We further added different concentrations of MurNAc-6-P and GlcNAc-6-P to the reaction system and monitored the fluorescence intensity. The addition of MurNAc-6-P significantly recovered the fluorescence of eGFP, while the addition of GlcNAc-6-P made

no visible difference (Figure 5C, E and Supplementary Figure S17 B and C). In addition, we introduced the K159A, H171A and K195A mutations (KHK) as well as the S146A, S190A and S192A (SSS) mutations into the MurR protein, creating KHK and SSS mutant MurR proteins. Both mutant proteins could normally bind to the DNA but failed to respond to MurNAc-6-P (Figure 5 D and E). Taken together, in the tested conditions, MurNAc-6-P, but not GlcNAc-6-P, could alleviate the binding of MurR with the operator DNA. In addition, ligand-binding residues are essential for ligand recognition.

We further assessed the impact of the mutations of the key residues *in vivo* by using growth curve assay. The S146A, K159A, H171A, S190A, S192A and K195A mutations were introduced into *E. coli* chromosomal DNA by homologous recombination and these mutants were then subjected to the growth curve assay. The growth of all six mutants was impaired in MMA-MurNAc medium compared with that of the WT strain (Figure 5F), probably because MurNAc-6-P could not lessen the inhibitory effect of the mutant MurR proteins; thus, the expression level of *murQP* in the mutant strains was lower than that in the WT strain, resulting in insufficient nutrients in the mutant strains for growth. Consistently, all nine strains grew at nearly the same speed in MMA-GlcNAc medium (Figure 5G). Together, these results demonstrated that the precise interaction between MurR and MurNAc-6-P is essential for the regulatory activity of MurR.

DISCUSSION

Cell wall recycling is vital for the recovery of resources and plays a pivotal role in antibiotic resistance in some bacterial species. In *E. coli*, the tetrameric MurR controls the expression of MurQ, MurP and itself via the signal molecule MurNAc-6-P, which is the intermediate product of cell-wall recycling. In this study, we demonstrated that MurNAc-6-P induces the dissociation of MurR from the promoter DNA by directly binding with MurR. In addition, we crystallized and solved the structure of MurR in complex with MurNAc-6-P, revealing the intricate network of contacts that mediate MurNAc-6-P recognition by MurR. According to the structure of the MurR/MurNAc-6-P complex, the key residues contributing to ligand binding were identified and their pivotal role in the regulatory activity of MurR was verified by *in vitro* and in cell assays.

Previous studies showed that other intermediates of amino sugar metabolism, such as GlcNAc, MurNAc, GlcNAc-6-P, anhydroMurNAc and muramyl dipeptide, had no effect on MurR binding to the operator site (39). In our work, GlcNAc-6-P was found to interact with MurR via direct binding, which disturbed the MurR-DNA interaction. However, due to the weaker interactions between MurR and GlcNAc-6-P, the regulatory capacity of GlcNAc-6-P was much lower than that of MurNAc-6-P, as confirmed by the *in vitro* and in cell assays. We also obtained the structure of MurR in complex with GlcNAc-6-P. Structural analysis revealed that K159 contacts MurNAc-6-P through a direct hydrogen bond while K159 forms a water-mediated hydrogen bond with GlcNAc-6-P. Together with the weaker interactions offered by L143, G145, H171, S244 and T281, GlcNAc-6-P shows weaker binding to MurR compared with that of MurNAc-6-P. The discrepancy in the binding affinity probably allows MurNAc-6-P, but not GlcNAc-6-P, to cause MurR to dissociate from the promoter DNA in cells.

The RpiR/AlsR family transcriptional regulator is conserved in a series of Gram-negative and Gram-positive bacteria, such as *Escherichia coli*, *Shigella dysenteriae*, *Citrobacter koseri*, *Staphylococcus aureus*, *Bacillus subtilis* and *Streptomyces coelicolor*. Nevertheless, this family was poorly characterized. To our knowledge, to date, only 5 crystal structures of the RpiR/AlsR family have been released, including the N-terminal domain of a RpiR transcriptional regulator from *Staphylococcus epidermidis* (PDB ID: 3IWF), the N-terminal domain of the putative transcriptional regulator ybbH from *Bacillus subtilis* (PDB ID: 2O3F), the sugar isomerase domain of a RpiR transcription factor from *Sphaerobacter thermophilus* (PDB ID: 3SHO), the *Vibrio vulnificus* NanR protein in complex with ManNAc-6P (PDB ID: 4IVN) and a putative phosphoheptose isomerase from *Bacillus halodurans* (PDB ID: 3CVJ). Among them, there is only one protein/ligand complex crystal structure, named NanR/ManNAc-6-P (48). As a member of the RpiR/AlsR family transcriptional regulators, MurR shares a 25% identity and a 51% positive amino acid sequence with NanR, which makes them highly superimposed LBD structures (1.243-Å rmsd, Supplementary Figure S18A). Similarly, MurR shares 22% identity and 43% positivity with 3SHO (1.309-Å rmsd, Supplementary Figure S18B). We performed a sequence alignment of MurR with its family members and found that the S146, H171, S190 and S192 residues were highly conserved (Supplementary Figure S19). S146, S190 and S192 directly interact with the phosphate group of MurNAc-6-P, indicating that the RpiR/AlsR family proteins might recognize phosphorylated cellular metabolites.

ACCESSION NUMBERS

The crystal structures of apo MurR, MurR/GlcNAc-6-P and MurR/MurNAc-6-P have been deposited in the RCSB Protein Data Bank (www.wwpdb.org) under the accession codes 7EN6, 7EN5 and 7EN7, respectively.

SUPPLEMENTARY DATA

Supplementary Data are available at NAR Online.

ACKNOWLEDGEMENTS

We thank staffs from BL19U1 beamline of National Facility for Protein Science Shanghai at Shanghai Synchrotron Radiation Facility for assistance during data collection.

FUNDING

National Natural Science Foundation of China [91753127, 21922705, 22077083 to Q.J., 21907066 to W.C.]; Lingang Laboratory [LG-QS-202206-05 to Q.J.]; Shanghai Science and Technology Committee [22ZR1480100 to Q.J., 19JC1410300 to S.Y.Z.]. Funding for open access charge: National Natural Science Foundation of China.
Conflict of interest statement. None declared.

REFERENCES

1. Vollmer,W. and Bertsche,U. (2008) Murein (peptidoglycan) structure, architecture and biosynthesis in *Escherichia coli*. *Biochim. Biophys. Acta.*, **1778**, 1714–1734.
2. Matias,V.R. and Beveridge,T.J. (2007) Cryo-electron microscopy of cell division in *Staphylococcus aureus* reveals a mid-zone between nascent cross walls. *Mol. Microbiol.*, **64**, 195–206.
3. Matias,V.R., Al-Amoudi,A., Dubochet,J. and Beveridge,T.J. (2003) Cryo-transmission electron microscopy of frozen-hydrated sections of *Escherichia coli* and *Pseudomonasaeruginosa*. *J. Bacteriol.*, **185**, 6112–6118.
4. Salton,M.R. (1953) Studies of the bacterial cell wall. IV. The composition of the cell walls of some Gram-positive and Gram-negative bacteria. *Biochim. Biophys. Acta.*, **10**, 512–523.
5. Schleifer,K.H. and Kandler,O. (1972) Peptidoglycan types of bacterial cell walls and their taxonomic implications. *Bacteriol. Rev.*, **36**, 407–477.
6. Perkins,H.R. (1963) Chemical structure and biosynthesis of bacterial cell walls. *Bacteriol. Rev.*, **27**, 18–55.
7. Vollmer,W., Blanot,D. and de Pedro,M.A. (2008) Peptidoglycan structure and architecture. *FEMS Microbiol. Rev.*, **32**, 149–167.
8. Vollmer,W., Joris,B., Charlier,P. and Foster,S. (2008) Bacterial peptidoglycan (murein) hydrolases. *FEMS Microbiol. Rev.*, **32**, 259–286.
9. Glauner,B., Höltje,J.V. and Schwarz,U. (1988) The composition of the murein of *Escherichia coli*. *J. Biol. Chem.*, **263**, 10088–10095.
10. Sauvage,E., Kerff,F., Terrak,M., Ayala,J.A. and Charlier,P. (2008) The penicillin-binding proteins: structure and role in peptidoglycan biosynthesis. *FEMS Microbiol. Rev.*, **32**, 234–258.
11. Goodell,E.W. (1985) Recycling of murein by *Escherichia coli*. *J. Bacteriol.*, **163**, 305–310.
12. Doyle,R.J., Chaloupka,J. and Vinter,V. (1988) Turnover of cell walls in microorganisms. *Microbiol. Rev.*, **52**, 554–567.
13. Jacobs,C., Huang,L.J., Bartowsky,E., Normark,S. and Park,J.T. (1994) Bacterial cell wall recycling provides cytosolic muropeptides as effectors for beta-lactamase induction. *EMBO J.*, **13**, 4684–4694.
14. Johnson,J.W., Fisher,J.F. and Mobashery,S. (2013) Bacterial cell-wall recycling. *Ann. N. Y. Acad. Sci.*, **1277**, 54–75.
15. Fisher,J.F. and Mobashery,S. (2014) The sentinel role of peptidoglycan recycling in the β-lactam resistance of the Gram-negative *Enterobacteriaceae* and *Pseudomonas aeruginosa*. *Bioorg. Chem.*, **56**, 41–48.
16. Tsuchido,T. and Takano,M. (1988) Sensitization by heat treatment of *Escherichiacoli* K-12 cells to hydrophobic antibacterial compounds. *Antimicrob. Agents Chemother.*, **32**, 1680–1683.
17. van Heijenoort,J. (2011) Peptidoglycan hydrolases of *Escherichiacoli*. *Microbiol. Mol. Biol. R.*, **75**, 636–663.
18. Heidrich,C., Templin,M.F., Ursinus,A., Merdanovic,M., Berger,J., Schwarz,H., de Pedro,M.A. and Höltje,J.V. (2001) Involvement of *N*-acetylmuramyl-L-alanine amidases in cell separation and antibiotic-induced autolysis of *Escherichia coli*. *Mol. Microbiol.*, **41**, 167–178.
19. Priyadarshini,R., de Pedro,M.A. and Young,K.D. (2007) Role of peptidoglycan amidases in the development and morphology of the division septum in *Escherichia coli*. *J. Bacteriol.*, **189**, 5334–5347.
20. Uehara,T. and Park,J.T. (2007) An anhydro-*N*-acetylmuramyl-L-alanine amidase with broad specificity tethered to the outer membrane of *Escherichia coli*. *J. Bacteriol.*, **189**, 5634–5641.
21. Scheurwater,E., Reid,C.W. and Clarke,A.J. (2008) Lytic transglycosylases: bacterial space-making autolysins. *Int. J. Biochem. Cell B.*, **40**, 586–591.
22. Cheng,Q. and Park,J.T. (2002) Substrate specificity of the AmpG permease required for recycling of cell wall anhydro-muropeptides. *J. Bacteriol.*, **184**, 6434–6436.
23. Jacobs,C., Joris,B., Jamin,M., Klarsov,K., Van Beeumen,J., Mengin-Lecreulx,D., van Heijenoort,J., Park,J.T., Normark,S. and Frère,J.M. (1995) AmpD, essential for both beta-lactamase regulation and cell wall recycling, is a novel cytosolic *N*-acetylmuramyl-L-alanine amidase. *Mol. Microbiol.*, **15**, 553–559.
24. Cheng,Q., Li,H., Merdek,K. and Park,J.T. (2000) Molecular characterization of the beta-*N*-acetylglucosaminidase of *Escherichiacoli* and its role in cell wall recycling. *J. Bacteriol.*, **182**, 4836–4840.
25. Vötsch,W. and Templin,M.F. (2000) Characterization of a beta -*N*-acetylglucosaminidase of *Escherichiacoli* and elucidation of its role in muropeptide recycling and beta-lactamase induction. *J. Biol. Chem.*, **275**, 39032–39038.
26. Uehara,T., Suefuji,K., Valbuena,N., Meehan,B., Donegan,M. and Park,J.T. (2005) Recycling of the anhydro-*N*-acetylmuramic acid derived from cell wall murein involves a two-step conversion to *N*-acetylglucosamine-phosphate. *J. Bacteriol.*, **187**, 3643–3649.
27. Bacik,J.P., Whitworth,G.E., Stubbs,K.A., Yadav,A.K., Martin,D.R., Bailey-Elkin,B.A., Vocadlo,D.J. and Mark,B.L. (2011) Molecular basis of 1,6-anhydro bond cleavage and phosphoryl transfer by *Pseudomonasaeruginosa* 1,6-anhydro-*N*-acetylmuramic acid kinase. *J. Biol. Chem.*, **286**, 12283–12291.
28. Dahl,U., Jaeger,T., Nguyen,B.T., Sattler,J.M. and Mayer,C. (2004) Identification of a phosphotransferase system of *Escherichiacoli* required for growth on *N*-acetylmuramic acid. *J. Bacteriol.*, **186**, 2385–2392.
29. Jaeger,T., Arsic,M. and Mayer,C. (2005) Scission of the lactyl ether bond of *N*-acetylmuramic acid by *Escherichiacoli* "etherase". *J. Biol. Chem.*, **280**, 30100–30106.
30. Hadi,T., Dahl,U., Mayer,C. and Tanner,M.E. (2008) Mechanistic studies on *N*-acetylmuramic acid 6-phosphate hydrolase (MurQ): an etherase involved in peptidoglycan recycling. *Biochemistry*, **47**, 11547–11558.
31. Plumbridge,J. (2009) An alternative route for recycling of *N*-acetylglucosamine from peptidoglycan involves the *N*-acetylglucosamine phosphotransferase system in *Escherichiacoli*. *J. Bacteriol.*, **191**, 5641–5647.
32. Park,J.T. and Uehara,T. (2008) How bacteria consume their own exoskeletons (turnover and recycling of cell wall peptidoglycan). *Microbiol. Mol. Biol. R.*, **72**, 211–227.
33. Barreteau,H., Kovac,A., Boniface,A., Sova,M., Gobec,S. and Blanot,D. (2008) Cytoplasmic steps of peptidoglycan biosynthesis. *FEMS Microbiol. Rev.*, **32**, 168–207.
34. Mengin-Lecreulx,D. and van Heijenoort,J. (1994) Copurification of glucosamine-1-phosphate acetyltransferase and *N*-acetylglucosamine-1-phosphate uridyltransferase activities of *Escherichiacoli*: characterization of the *glmU* gene product as a bifunctional enzyme catalyzing two subsequent steps in the pathway for UDP-*N*-acetylglucosamine synthesis. *J. Bacteriol.*, **176**, 5788–5795.
35. Benson,T.E., Marquardt,J.L., Marquardt,A.C., Etzkorn,F.A. and Walsh,C.T. (1993) Overexpression, purification, and mechanistic study of UDP-*N*-acetylenolpyruvylglucosamine reductase. *Biochemistry*, **32**, 2024–2030.
36. Bouhss,A., Crouvoisier,M., Blanot,D. and Mengin-Lecreulx,D. (2004) Purification and characterization of the bacterial MraY translocase catalyzing the first membrane step of peptidoglycan biosynthesis. *J. Biol. Chem.*, **279**, 29974–29980.
37. Mengin-Lecreulx,D., Texier,L., Rousseau,M. and van Heijenoort,J. (1991) The *murG* gene of *Escherichiacoli* codes for the UDP-*N*-acetylglucosamine: *N*-acetylmuramyl-(pentapeptide) pyrophosphoryl-undecaprenol *N*-acetylglucosamine transferase involved in the membrane steps of peptidoglycan synthesis. *J. Bacteriol.*, **173**, 4625–4636.
38. Pomorski,T. and Menon,A.K. (2006) Lipid flippases and their biological functions. *Cell. Mol. Life Sci.*, **63**, 2908–2921.
39. Jaeger,T. and Mayer,C. (2008) The transcriptional factors MurR and catabolite activator protein regulate *N*-acetylmuramic acid catabolism in *Escherichiacoli*. *J. Bacteriol.*, **190**, 6598–6608.
40. Jiang,W., Bikard,D., Cox,D., Zhang,F. and Marraffini,L.A. (2013) RNA-guided editing of bacterial genomes using CRISPR-Cas systems. *Nat. Biotechnol.*, **31**, 233–239.
41. Datsenko,K.A. and Wanner,B.L. (2000) One-step inactivation of chromosomal genes in *Escherichiacoli* K-12 using PCR products. *Proc. Natl. Acad. Sci. U.S.A.*, **97**, 6640–6645.
42. Yamaguchi,T., Hesek,D., Lee,M., Oliver,A.G. and Mobashery,S. (2010) Sulfonylation-induced *N*- to *O*-acetyl migration in 2-acetamidoethanol derivatives. *J. Org. Chem.*, **75**, 3515–3517.
43. Bera,S. and Linhardt,R.J. (2011) Design and synthesis of unnatural heparosan and chondroitin building blocks. *J. Org. Chem.*, **76**, 3181–3193.

44. Wohnig,S., Spork,A.P., Koppermann,S., Mieskes,G., Gisch,N., Jahn,R. and Ducho,C. (2016) Total synthesis of dansylated park's nucleotide for high-throughput MraY assays. *Chem. Eur. J.*, **22**, 17813–17819.
45. Kumar,S.C., Rodrigo,S.P., Harald,B., Maxence,D. and Catherine,A.G.J.B. (2020) FlaGs and webFlaGs: discovering novel biology through the analysis of gene neighbourhood conservation. *Bioinformatics*, **37**, 1312–1314.
46. Liu,W.Q., Wu,C., Jewett,M.C. and Li,J. (2020) Cell-free protein synthesis enables one-pot cascade biotransformation in an aqueous-organic biphasic system. *Biotechnol. Bioeng.*, **117**, 4001–4008.
47. Zhuang,L., Huang,S., Liu,W.Q., Karim,A.S., Jewett,M.C. and Li,J. (2020) Total in vitro biosynthesis of the nonribosomal macrolactone peptide valinomycin. *Metab. Eng.*, **60**, 37–44.
48. Hwang,J., Kim,B.S., Jang,S.Y., Lim,J.G., You,D.J., Jung,H.S., Oh,T.K., Lee,J.O., Choi,S.H. and Kim,M.H. (2013) Structural insights into the regulation of sialic acid catabolism by the *Vibriovulnificus* transcriptional repressor NanR. *Proc. Natl. Acad. Sci. U.S.A.*, **110**, E2829–E2837.